

# Mechanical Design of a ReBCO Non/Metal-Insulated 40 T Solenoid for the Muon Collider

C. Accettura , A. Bertarelli , B. Bordini , L. Bottura , A. Dudarev , A. Kolehmainen, T. Mulder , F. Sanda, and G. Vernassa 

**Abstract**—In the framework of the design studies of a Muon Collider (MuC), the design of Ultra-High-Field (UHF) magnets is a crucial part, particularly for the MuC’s final cooling stage. To address this, CERN has recently introduced a conceptual design for a 40 T solenoid characterized by very compact pancake coils. Due to the high magnetic field and operating current density (approximately 600 A/mm<sup>2</sup>), the Lorentz forces acting on the winding are extremely large. Consequently, the mechanical design, along with quench protection, represents a significant challenge in the development of this magnet. An additional mechanical complexity is constituted by the strong anisotropy and low strength of ReBCO tapes. This article focuses on the proposed mechanical design of the 40 T solenoid. The primary objective of this design is to keep the stresses induced in the coils by Lorentz forces below materials admissible limits. Initially, the paper presents a conceptual design based on analytical calculations relying on the application of a radial pre-compression (approximately 200 MPa) to the pancake coils by shrink-fitting, prior to energization. Subsequently, a finite element analysis is performed, introducing various nonlinearities (material, geometric, plasticity) to optimize the magnet’s design. The study also investigates a hybrid solution, in which the initial coil loading is obtained by a combination of shrink fitting and mechanical compression by a clamped conical connection based on shrink discs. The highly anisotropic mechanical properties of the tape, which are not extensively documented in current literature, were investigated by a series of dedicated tests relying on specially designed tooling. This design and experimental testing complement the simulation efforts by allowing to derive and implement in the models more accurate material properties. In conclusion, the proposed magnet design exemplifies a synergistic integration of experimental work and simulation efforts, advancing the development of UHF magnets for the Muon Collider.

**Index Terms**—Muon-collider, ReBCO, solenoid, ultra-high-field.

## I. INTRODUCTION

THE Muon Collider (MuC) is being considered as one of the potential successors to the Large Hadron Collider (LHC) at CERN. The muons, which have a mass 207 times greater than the electrons, experience significantly lower synchrotron radi-

ation losses, making them well-suited for high-energy circular accelerator. Protons, while possessing even greater mass, are not elementary particles. Their internal structure complicates the interpretation of collision results. However, muons are unstable particles with a very short lifetime (2.2 s at rest), presenting unique challenges for beam cooling and acceleration [1].

A key component of the MuC is the final cooling channel, which aims to reduce the transverse emittance of the muons to improve beam quality [2]. The final cooling channel consists of multiple cells, each featuring one ultra-high-field solenoid that focuses the muon beam, alongside liquid hydrogen absorbers and RF cavities for energy-phase rotation. These solenoids are critical for minimizing both transverse and longitudinal emittance, allowing the beam to be efficiently accelerated. Achieving the required cooling in this stage demands solenoids capable of generating magnetic fields above 40 T with requirements for field homogeneity and mechanical stability.

Currently, two main approaches are used to create ultra-high field solenoids [3]. The first involves hybrid magnets, combining superconducting Nb<sub>3</sub>Sn coils with resistive inserts to generate fields above 40 T, but this requires high power consumption (usually over 20 MW). The second approach uses fully superconducting magnets made from Nb-Ti, Nb<sub>3</sub>Sn, and high-temperature superconductors (HTS) like ReBCO, which reduce mechanical stress by distributing the ampere-turns across thick nested coils powered independently. However, this method increases tape consumption, leading to higher costs, larger sizes, and construction challenges, limiting its application in particle accelerators. In contrast to these techniques, our design proposes a modular, non-insulated (NI) ReBCO HTS solenoid operated at high current density aimed at overcoming these challenges and optimizing the final cooling process for the MuC.

In this paper, we examine one of the most critical aspects of this design: the management of mechanical stresses. The high magnetic fields required for the final cooling solenoids impose significant mechanical stress on the conductor.

The remainder of the paper is structured as follows: first, the conceptual design of the magnet is reviewed. Next, the mechanical design is addressed analytically, using simplified formulas to estimate dimensions. A finite element model (FEM) is then introduced to account for nonlinearities and provide a more complete analysis. Finally, considerations related to the component’s manufacturing are discussed.

Received 1 October 2024; revised 7 November 2024; accepted 13 November 2024. Date of publication 21 November 2024; date of current version 18 December 2024. This work was supported by the European Union (EU). (Corresponding author: C. Accettura.)

The authors are with the European Organization for Nuclear Research (CERN), 1211 Geneva, Switzerland (e-mail: carlotta.accettura@cern.ch).

Color versions of one or more figures in this article are available at <https://doi.org/10.1109/TASC.2024.3504472>.

Digital Object Identifier 10.1109/TASC.2024.3504472

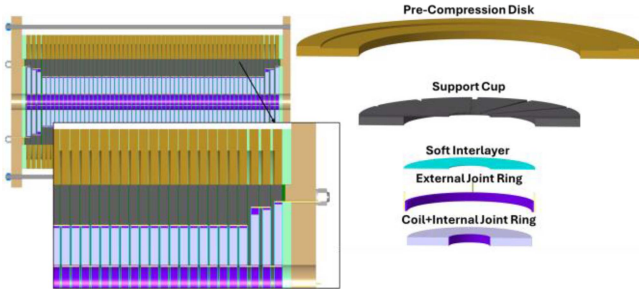


Fig. 1. Magnet assembly (left) and radial building of a pancake (right).

## II. CONCEPTUAL DESIGN

The compact full HTS design operated at high current density ( $500 \text{ A/mm}^2$ ) is based on the goal of minimizing conductor usage and reducing system complexity while optimizing space efficiency and lowering overall footprint. However, this approach results in a design where managing mechanical stress induced by Lorentz forces becomes a central focus. When operating at high magnetic fields, it is crucial to account for the magnetic pressure  $P_M$  developed in the coil [3], which can be calculated as shown in (1).

$$P_M = \frac{B^2}{2 \cdot \mu_0} \quad (1)$$

Where  $\mu_0$  is the magnetic permeability of the free space and  $B$  is the magnetic flux density.

At 40 T, the  $P_M$  reaches 640 MPa. For a compact coil, the maximum hoop stress is approximately 1.4–2.2 times  $P_M$  [3], thus we would obtain a hoop stress of 1300 MPa at the coil's inner radius. Assuming the limit of applied hoop strain to prevent critical current degradation is between 0.4–0.5% [4], the maximum acceptable hoop stress would range between 600 and 950 MPa. This range results from the varying values of critical strain reported in the literature and the copper thickness in the tape, which affects the coil's stiffness and, consequently, its response to the applied force. To limit tensile hoop stresses in operation within this range, the coil must be pre-compressed.

The conceptual design of the superconducting magnet is based on several key aspects:

**Superconductor:** The design employs 12 mm-wide ReBCO tape as superconductor, given its excellent performance in high magnetic fields and at low operating temperatures (4.2 K) [5].

**Pancake Coil:** Adjacent turns are soldered. The inner turn is soldered to its Internal Joint Ring, and the outer turn is soldered to its External Joint Ring. The Inner Radius ( $r_{i,coil}$ ) of the coil winding is 30 mm and its Outer Radius ( $r_{e,coil}$ ) is 90 mm.

**Geometrical Layout:** The magnet design consists of a series of identical modular pancake coils and correction coils, as shown in Fig.1. Each pancake is surrounded by a support cup, which consists of a 12 mm high disk and a 1.5 mm thick radial plate that alternates between adjacent pancakes. A pre-compression disk is the final component of the magnet radial building [6].

In this paper, we describe the mechanical aspects which led to this configuration. Electromagnetic design is presented elsewhere [6].

## III. MECHANICAL DESIGN

The initial sizing of the mechanical pre-compression system was performed analytically through the theory of plane axisymmetric problems. The basic concept involves applying pre-compression through thermally induced shrink fitting. The pre-compression must generate a compressive hoop stress of approximately 500 MPa at the inner radius  $r_{i,coil}$  of the coil to ensure that the stress remains below the 800 MPa limit when  $P_M$  induces a stress of 1300 MPa. If we consider a thick cylinder representing the coil submitted to external pressure  $p_e$ , the hoop stress can be calculated with (2) [7].

$$\sigma_\theta(r) = -\frac{p_e \cdot r_{e,coil}^2 \left(1 + \frac{r_{i,coil}^2}{r^2}\right)}{r_{e,coil}^2 - r_{i,coil}^2} \quad (2)$$

Thus, to achieve the required pre-compression with the given coil dimensions, an external pressure exceeding 220 MPa is necessary, regardless of the coil's elastic modulus. Such pre-compression can be obtained by the shrink-fitting effect of an outer thick shell. The idea involves heating a shell with inner radius  $r_{i,shell}$  lower than the  $r_{e,coil}$  and assembling it around the coil. Upon cooling, the contraction of the shell exerts an external radial pressure, which would help achieve the desired pre-compression by interference. The relation between the  $p_e$  and  $\delta$  can also be calculated analytically according to (3) [7].

$$\delta = \left[ \frac{1}{E_{shell}} \left( \frac{1 + \beta_{shell}^2}{1 - \beta_{shell}^2} + \nu_{shell} \right) + \frac{1}{E_{coil}} \left( \frac{1 + \beta_{coil}^2}{1 - \beta_{coil}^2} + \nu_{coil} \right) \right] \cdot r_{e,coil} \cdot p_e \quad (3)$$

where  $E_{shell}$  and  $E_{coil}$  are the Young's moduli,  $\beta_{shell}$  and  $\beta_{coil}$  are the Poisson's ratio, and  $\nu$  is the ratio of  $r_e$  to  $r_i$  of the shell and coil. For the shell, a generic steel with  $E_{shell}$  210 GPa and  $\beta_{shell}$  0.29 is considered. For the coil, by applying the rule of mixtures, we obtain  $E_{coil}$  180 GPa and  $\beta_{coil}$  0.30.

The required pressure  $P_M$  220 MPa is achieved with an interference of approximately 250  $\mu\text{m}$ . If we neglect the differential thermal contraction between coil and shell down to 4.2K, this interference is solely due to the thermal contraction of the shell as it cools to room temperature, which can be estimated using (4).

$$\delta = \alpha \cdot \Delta T \cdot r_{i,shell} \quad (4)$$

To achieve the necessary contraction, a temperature difference  $\Delta T$  of 170 °C is required. With the same formula, we can also calculate the coil and shell thermal contraction down to 4.2K. In this case, we should consider an equivalent contraction of the coil based on its composition.

This preliminary calculation serves to verify whether the proposed concept is feasible and ensures that the required temperatures do not exceed the maximum allowable for the ReBCO tape. It is also important because it gives an initial estimate of the outer

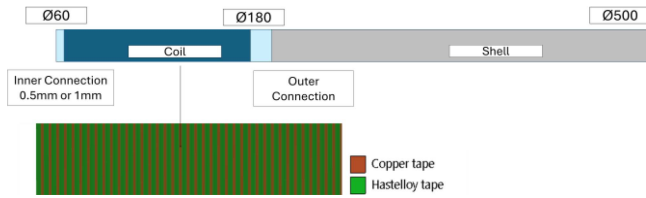


Fig. 2. Geometrical model of a single pancake. The inner, outer layer and the coil are model with 30 m of copper and 50 m of Hastelloy.

shell dimensions. In these calculations, we assumed a  $r_{e,shell}$  of 250 mm, as a smaller shell would be less rigid and would require higher temperatures to achieve the same compression. Using this approach, and exploiting the same formula shown in (3), we can also estimate how much the precompression may be affected by tolerances, which were not considered in this calculation. Specifically, we lose approximately 1 MPa in contact pressure per m of interference deviation.

#### IV. 2D FINITE ELEMENT ANALYSIS

For a complete assessment of the magnet's mechanical behavior, a FEM is required to address various non-linearities, including material properties and frictional contacts. Additionally, it is essential to account for the contributions of the inner and external joint rings. Initially, the analysis focuses on a single pancake to simplify the evaluation and gain insight into the critical aspects of stress distribution and deformation.

##### A. Geometry

The initial analysis is conducted using a 2D axially symmetric model in ANSYS workbench. The internal and external joint, which are required for the electrical connection between the pancakes, are made from the same materials as the tape (copper and Hastelloy) without the ReBCO layer. This design choice was taken after several optimizations aimed at minimizing the stresses resulting from differential thermal contraction during the magnet cool-down.

The results presented were obtained using an internal joint thickness ranging from 0.5 to 1 mm, while the outer extended up to 6 mm. The tape is represented as consisting of 30m of copper and 50m of Hastelloy, wound into a multi-turn structure to form the coil, as shown in Fig.2.

##### B. Material Models

The copper and Hastelloy elastic properties are considered at room temperature (RT) and at 77K [4]. For the shell, we initially considered the Stainless Steel 304 [8]. The values are summarized in Table I. The secant coefficient of thermal expansion (CTE) is shown in Fig.3 [9], [10]. Hastelloy is approximated with Inconel 718. For Hastelloy an isotropic elastic model is used, while for copper a multilinear isotropic hardening rule was assumed [4]. The resulting true stress-plastic strain curves are plotted in Fig.4.

TABLE I  
MATERIAL ELASTIC PROPERTIES

T(°C)	$E_{cu}$ (GPa)	$E_{Ha}$ (GPa)	$E_{Shell}$ (GPa)
-263	98	228	210
22	8	223	200
T(°C)	$\nu_{cu}$	$\nu_{Ha}$	$\nu_{Shell}$
-263	0.34	0.30	0.27
22	0.34	0.30	0.27

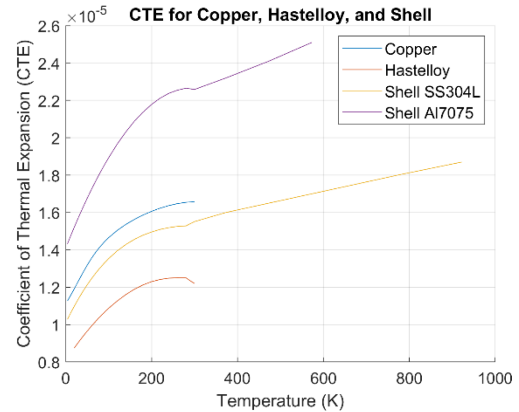


Fig. 3. Material secant CTE.

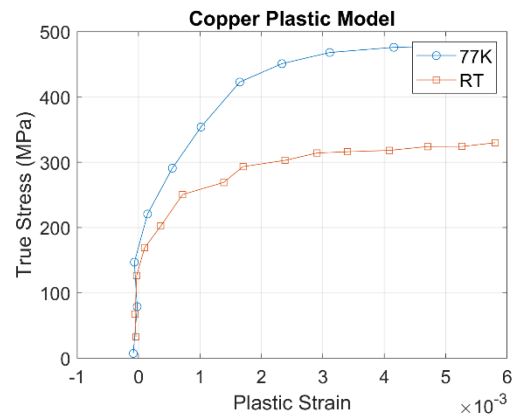


Fig. 4. Copper plastic model.

##### C. Boundary Conditions and Loads

The analysis is divided into three steps:

- Step 1: External shell cooling from 200°C down to room temperature.
- Step 2: System cooling down to -10K.
- Step 3: Magnet energization.

The magnetic forces  $F(r) = B(r) \cdot J$  are calculated with the following simplification:

$$\text{Constant current density } J = \frac{B_{\max}}{\mu_0(r_{e,coil} - r_{i,coil})}$$

$$\text{Linear field } B(r) = \mu_0 \cdot J \cdot (r - r_{i,coil}).$$

The magnetic field  $B$  is assumed to be parallel to the solenoid's axis.

The resulting peak force density is 23Nmm<sup>-3</sup>.

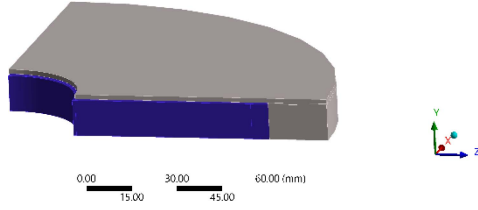


Fig. 5. 3D of the pancake with the support cup.

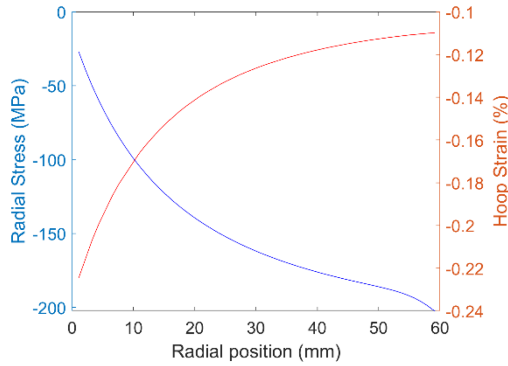


Fig. 6. Radial stress (blue) and hoop strain (red) in step 1. The radial position is measured from the coil inner radius. Thus, the origin corresponds to a distance from the coil axis of 30mm.

Frictionless support is applied on the first two layers of the internal joint to consider the supporting system.

## V. FABRICATION ASSEMBLY ANALYSIS

Once the 2D model and the design of the electrical joints are validated, the effects of other components are introduced. First, the 1.5 mm plate that separates axially the individual pancakes needs to be included. This plate, that intercepts the axial forces coming from the magnet head [6], is attached to the first compression disk. In this study, an outer radius of approximately 110 mm is used for the first compression disk, while the remaining compression is applied via an external disk with a diameter of 250 mm. However, it is important to note that this optimization is still in progress and has not yet been finalized. This model is analyzed in 3D to explore different disk configurations, as shown in Fig. 5.

## VI. RESULTS AND DISCUSSION

Using the 2D FEM analysis, we can evaluate the stress and strain in all elements. In the first step, we confirm that the analytical results hold true, and the required pre-compression of 200MPa is achieved on the external layer of the coil, as shown in Fig.6. However, during the cooldown, some of this pre-compression is lost due to differential thermal contraction, which is slightly higher for the coil because of its Cu content, as visible in Fig.7. It is also important to assess shear stresses, as they could severely affect tape functionality [6]. The peak of 5MPa is localized in the vicinity of the external joint, but it remains below the limit of 10MPa [6].

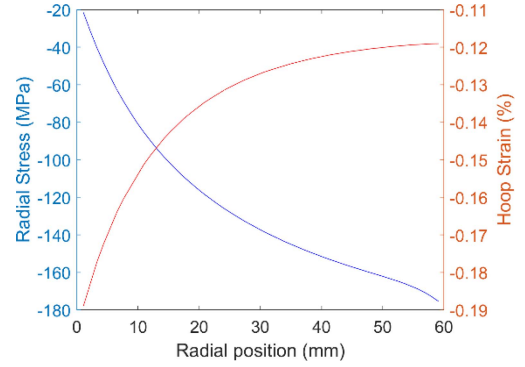


Fig. 7. Radial stress and hoop strain in step 2.

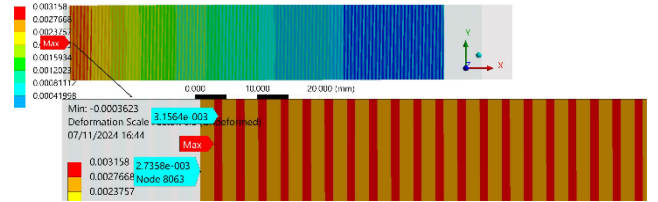
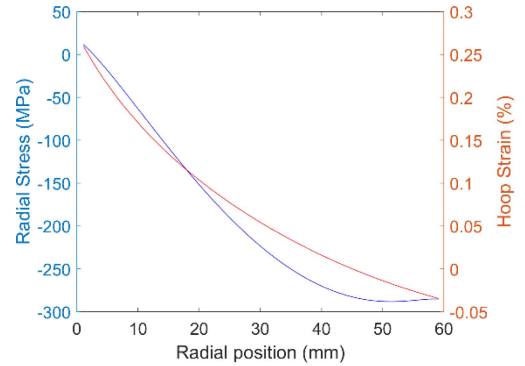
Fig. 8. Elastic  $\epsilon_{\theta}$  in copper and hastelloy.

Fig. 9. Radial stress and hoop strain in step 3.

In the third stage, we examine the hoop strain  $\epsilon_{\theta}$ . In a multi-layer system composed of different materials, such as copper, Hastelloy, and ReBCO, the total strain (both elastic and thermal) must remain continuous across all layers to maintain mechanical compatibility. However, the elastic strain distribution, which is key to assessing the performance of the ReBCO layer particularly in terms of current degradation varies between the materials due to differences in their thermo-mechanical properties, as illustrated in Fig.8. To estimate the elastic strain in the ReBCO, we look at the Hastelloy, as it has properties (modulus of elasticity and thermal expansion) closer to ReBCO compared to copper.

With this configuration, a tensile radial stress of 10MPa is reached at the inner radius of the coil, as shown in Fig.9.

This effect can however be reduced by decreasing the thickness of the inner ring or by increasing the pre-heating temperature. This comparative study is shown in Table II, where the minimum is located at the outer radius, while the maximum is at the inner radius.

TABLE II  
STRESS AND STRAIN FOR DIFFERENT CONFIGURATION

Inner Joint ring thickness (mm)	Pre-compression at cold (MPa)	Radial stress (MPa)			Hoop Strain (%)		
		Step 1	Step 2	Step 3	Step 1	Step 2	Step 3
0.5	170	-205/-8	-190/-5	<b>-290/10</b>	-0.25/-0.10	-0.20/-0.12	-0.04/0.28
	250	-318/-12	-258/-8	<b>-367/7</b>	-0.39/-0.17	-0.31/-0.16	-0.09/0.18
1	170	-205/-14	-190/-10	<b>-288/19</b>	-0.25/-0.10	-0.2/-0.12	-0.05/0.29
	250	-320/-21	-259/-15	<b>-366/13</b>	-0.39/-0.17	-0.3/-0.16	-0.09/0.18

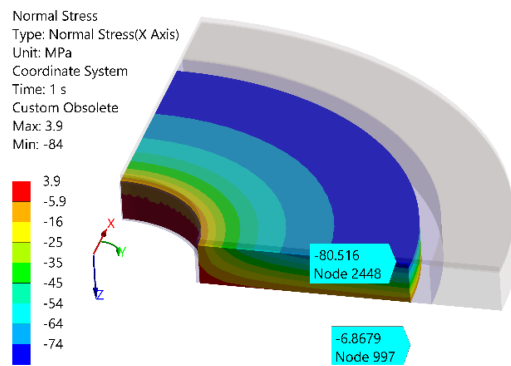


Fig. 10. Radial stress with the cup.

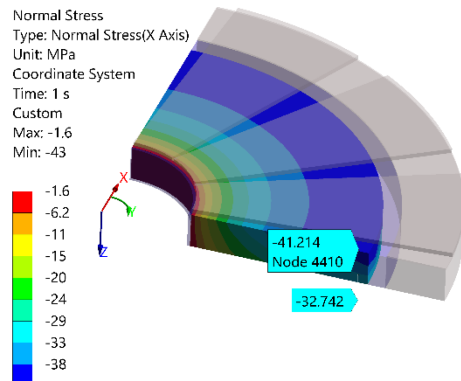


Fig. 11. Radial stress with the grooved cup.

It is important to note that these results are valid for the aforementioned material model. If we consider an elastic model also for copper, the hoop strain decreases to 0.25%.

From this analysis, the Von Mises stress on the external shell can also be obtained. On average, the stresses are around 200MPa, with peaks exceeding 500 MPa at the inner radius, thus necessitating the use of high-strength steel.

When the top plate is introduced, we immediately observe that during the shrink-fitting process, the protruding edge of the support cup induces an asymmetrical compression on the coil, resulting in flexure. This results in significant pressure non-uniformity, increasing the risk of exceeding critical stress levels once the magnet is energized, as shown in Fig.10. This

phenomenon is related to the stiffness of the disk. For this reason, an alternative version was tested. In this case, several radial grooves were added to reduce the circumferential stiffness of the disk, as shown in Fig.11. The grooves help distribute the forces more uniformly, mitigating the flexure observed in the original design.

## VII. CONCLUSION

The preliminary design and analysis of the 40 T ReBCO non-insulated solenoid for the Muon Collider demonstrate the mechanical feasibility of the thermal shrink fitting concept for pre-compression. The results indicate that a pre-compression of approximately 202 MPa can be achieved, ensuring that the hoop stresses in the coil remain within safe limits during magnet operation. The introduction of grooves in the compression disk effectively mitigates the issue of asymmetric loading and flexure, improving the uniformity of pressure distribution. These modifications are crucial for maintaining mechanical integrity under high magnetic fields.

This study highlights several areas that require further investigation, including material characterization, optimization of the shell stiffness, and reduction of manufacturing tolerances. Overall, the proposed design presents a promising solution for high-field solenoids in the final cooling stage of the Muon Collider, though additional refinements and testing are necessary to fully optimize the system.

## ACKNOWLEDGEMENT

Views and opinions expressed are however those of the author(s) only and do not necessarily reflect those of the EU or European Research Executive Agency (REA). Neither the EU nor the REA can be held responsible for them.

## REFERENCES

- [1] C. Aim et al., "Muon collider physics summary," 2022, *arXiv:2203.07256v2*.
- [2] D. Neuffer et al., "Final cooling for a high-energy high-luminosity lepton collider," *J. Instrum.*, vol. 12, 2017, Art.no. T07003.
- [3] B. Bordini et al., "Conceptual design of a ReBCO non/metal-insulated ultra-high field solenoid for the Muon Collider," *IEEE Trans. Appl. Supercond.*, vol. 34, no. 3, May 2024, Art.no. 4301310.
- [4] K. Ilin et al., "Experiments and FE modeling of stress-strain state in ReBCO tape under tensile, torsional, and transverse load," *Supercond. Sci. Technol.*, vol. 28, no. 5, 2015, Art.no. 055006.
- [5] S. Fujita et al., "Flux-pinning properties of BaHfO<sub>3</sub>-doped EuBCO-coated conductors fabricated by hot-wall PLD," *IEEE Trans. Appl. Supercond.*, vol. 29, no. 5, Aug. 2019, Art.no. 8001505, doi:10.1109/TASC.2019.2896535.
- [6] B. Bordini et al., "Development of a ReBCO non/metal-insulated 40 T solenoid for the Muon Collider," in *Proc. Appl. Supercond. Conf.*, 2024.
- [7] G. Petrucci, "Lezioni Di Costruzione di Macchine," Universita degli studi di Palermo, Didactic material.
- [8] National Institute of Standards and Technology (NIST), "Stainless steel properties," (n.d.). [Online]. Available: [https://trc.nist.gov/cryogenics/materials/304Stainless/304Stainless\\_rev.htm](https://trc.nist.gov/cryogenics/materials/304Stainless/304Stainless_rev.htm)
- [9] P. E. Bradley, "Properties of selected materials at cryogenic temperatures," 2013. [Online]. Available: [https://tsapps.nist.gov/publication/get\\_pdf.cfm?pub\\_id=913059](https://tsapps.nist.gov/publication/get_pdf.cfm?pub_id=913059)
- [10] "Stainless steel properties at high temperature," (n.d.). [Online]. Available: [https://swisssteel-group.com/content-media/documents/Data-Sheets/Stainless-Steel/1.4306\\_en.pdf](https://swisssteel-group.com/content-media/documents/Data-Sheets/Stainless-Steel/1.4306_en.pdf)